The Icing of an Unheated, Nonrotating Cylinder. Part I: A Simulation Model

E. P. LOZOWSKI,[1] J. R. STALLABRASS AND P. F. HEARTY

Low Temperature Laboratory, Division of Mechanical Engineering, National Research Council of Canada, Ottawa, Ontario, Canada K1A 0R6

(Manuscript received 23 February 1983, in final form 25 August 1983)

ABSTRACT

A model is described which simulates icing on an unheated, non-rotating cylinder. Both rime and glaze ice can be accounted for. The model computes the thermodynamic conditions and the initial icing rate as a function of angle around the upstream face of the cylinder. Although the model is not time-dependent, the initial icing rate can be used to compute local ice thickness after a specified time interval, and these in turn allow one to plot the ice accretion profile in either a single-step or multi-step fashion. Thus it is possible to predict total ice accretion cross-sectional area and mass for ice grown under varying conditions of airspeed, air temperature and pressure, cloud liquid water content, droplet size distribution, and cylinder size. Results are presented on the stagnation line growth rate as a function of liquid water content and airspeed, and examples of accretion profiles over a range of environmental conditions are provided. Although the model may be applied quite generally, the model results presented here are applicable to aircraft icing conditions.

1. Introduction

There is a need for models of the ice accretion process in several fields. The understanding and prediction of hail formation, power line icing, aircraft icing and marine icing are enhanced if models are available to help analyze and organize the physics, and to assist with the practical estimation of icing effects. In these and other fields the phenomenology of icing may be quite different because of differences in the geometry of the icing substrate, the sizes and chemical composition of the supercooled water droplets, ice crystals, or snow, and the ranges of liquid water content, air speed and air temperature involved. It is at present inconceivable that a single icing model could span the entire range of applications. Consequently, specific models have evolved in each of the fields. A few examples include those of Lozowski and d'Amours (1980) for hail, Lozowski and Oleskiw (1981) for airfoils, Stallabrass (1980) for fishing trawlers, and McComber (1982) for power lines.

Despite differences in detail, a unifying theme of most icing research seems to be that cylinder icing can be used either as a first approximation to the icing of the actual substrate of interest (e.g., power line conductors or ship masts and rigging), or as an initial estimate of icing effects which can be empirically or statistically related to the actual icing effects which one wishes to understand and predict. Thus the icing of cylinders is central to icing research in many fields. Ludlam (1951) was among the first to properly formulate a model for the icing of a rotating cylinder. Until now, the modeling of the icing of non-rotating cylinders has largely been limited either to a consideration of icing on the stagnation line (Stallabrass, 1957; Makkonen, 1981) or to a consideration of rime icing only (Ackley and Templeton, 1979).

The purpose of this paper is to extend the modeling for non-rotating cylinders to allow consideration of icing as a function of angle around the cylinder in both rime and glaze conditions. Cansdale and McNaughtan (1977) pointed the way but did not present results. In the present model, surface runback of water is considered and the shape of the resulting icing accretion is predicted. A major limitation of the model is that it is not time-dependent, so that feedback effects between the developing ice accretion and the air and droplet flows are not taken into account.

In Part I, we examine the model in detail and use it to make predictions of icing extent and shape on an unheated, non-rotating cylinder. In Part II, icing wind tunnel experiments are described and their results are compared with the model's predictions. Further details, including a computer listing of the model, are contained in Lozowski, Stallabrass and Hearty (1979).

Part of the reason for producing this series of papers is to make the material in this NRCC report more generally available to the various icing communities. It is the author's experience that many investigators in this field are unaware of important research results that have been obtained by others, because they are

[1] Present affiliation: Division of Meteorology, Department of Geography, University of Alberta, Edmonton, Alberta, Canada T6G 2H4.

written up in internal reports or other publications which are not widely distributed and may be difficult to obtain. Because the atmosphere is a common parameter in all of the types of icing we have alluded to, it seems appropriate that workers in this field might communicate with each other by publishing their most significant work in atmospheric science journals.

2. The model formulation

The situation under consideration is one in which an unheated, non-rotating cylinder of diameter D_c is located in a uniform airstream of velocity U far away from the cylinder. The airstream contains a cloud of supercooled water droplets, with a certain size spectrum and liquid water content w. The airstream and droplet cloud are assumed to be in thermodynamic and mechanical equilibrium, so that the droplets possess the air temperature t_a (°C) and they are moving with velocity U far away from the cylinder.

These are the macroscopic environmental conditions, which must be specified by the modeler. The formulation of the model consists of three parts: First the local impingement flux of supercooled water is computed as a function of position around the upstream surface of the cylinder. Second, the steady-state heat balance equation is solved, again as a function of position to determine the local surface temperature and the initial rate of ice accumulation. Finally, the rate of ice accumulation is used to forecast the local ice growth rate and thus the local thickness of ice after a specified time interval. By plotting these thicknesses around the cylinder, we can then determine the accretion shape and cross-sectional area or mass.

a. Droplet impingement

In order to determine the local rate of droplet impingement, one first discretizes the problem by dividing the upwind face of the cylinder into angular sectors, each 5° in width and centered on the angles $\theta_i = 5i°$, $i = 0, 1, 1, \cdots 18$. The droplet size spectrum is also discretized by dividing it into nine diameter categories, each 5 μm wide and centered on the diameters $D_j = 5j$ μm, $j = 1, 2, \cdots 9$. Droplets within each category are assumed to have the central diameter. Droplets larger than 45 μm in diameter are not allowed for in the model as it stands, although this could be changed quite easily if large droplets were present in the cloud in significant numbers.

For each angular sector i and droplet size category j the local collision efficiency, $\beta_{ij} = \beta_j(\theta_i)$ is calculated according to the formulas presented in Appendix A. This is defined as the ratio of the mass of water (in the jth droplet size category) actually impinging on the ith sector, to that which would be caught if the droplet trajectories were straight lines parallel to the undisturbed flow, and if the surface element were oriented perpendicular to the flow.

The overall collision efficiency for each sector is the mass-weighted mean for all the drop size categories, namely,

$$\beta_i = \beta(\theta_i) = \sum_j f_j \beta_{ij}, \tag{1}$$

where f_j is the fraction of the total water mass flux in the undisturbed flow, consisting of droplets in the jth size category. Finally, the liquid water mass flux impinging on each sector is given by

$$R_{wi} = \beta_i U w. \tag{2}$$

It is assumed in the model that the coalescence efficiency for the water droplets is unity and that there is no splashing. Thus, all the impinging water is assumed to adhere (although not necessarily at the point of impact), and consequently some of the effects observed by List (1977) at very high liquid water contents are not accounted for.

b. Steady-state heat balance

The steady-state heat balance equation that is assumed to describe the thermodynamics of the accretion may be written formally as (Messinger, 1953)

$$q_c + q_e + q_v + q_k + q_f + q_w + q_i + q_r + q_w^* + q_f^* = 0, \tag{3}$$

where

- q_c the sensible heat flux between the accretion and the airstream by conduction and convection,
- q_e the evaporative heat flux,
- q_v the heat flux due to aerodynamic heating,
- q_k the heat flux due to the conversion of droplet kinetic energy into heat,
- q_f the latent heat flux to the accretion due to freezing of some, or all, of the directly impinging water,
- q_w the sensible heat flux between the directly impinging water and the underlying accretion,
- q_i the heat flux between the accretion and the underlying surface,
- q_r the radiative heat flux between the accretion and the airstream,
- q_w^* similar to q_w but for runback water,
- q_f^* similar to q_f but for runback water.

All of the heat fluxes q are assumed to be positive if they *add* heat to the accretion, and negative in the opposite case. Eq. (3) is applied in each angular sector, beginning at the stagnation line and working outwards to $\theta = 90°$. We assume a horizontal cylinder with symmetry above and below the stagnation line. Any unfrozen water in one sector is assumed to be driven outwards and backwards by the airflow to the next downstream sector. This runback water then participates in the thermodynamics of the next sector through the two q^* terms. Eventually the runback water may

continue on past the maximum impingement angle, θ_m. In this way, very wet accretions may build up all the way to $\theta = 90°$. However, at 90° all remaining runback water is assumed to be shed into the airstream. In addition, this mechanism assumes that the airflow is strong enough to overcome the effects of gravity. There will obviously be some natural icing occurrences (freezing rain for instance) where gravitational effects on the unfrozen water will dominate the aerodynamic ones, and an asymmetric accretion can be expected. The model cannot simulate this type of accretion.

Let us now consider the detailed formulation of the terms in Eq. (3). We begin by ignoring the radiation and internal conduction terms q_r and q_i. This is done for simplicity, and because in certain instances of atmospheric icing, they will be negligible compared with the other terms. However, before applying the present model to a particular situation, one would do well to attempt to estimate these fluxes and ensure that they can be neglected (Lozowski and d'Amours, 1980; Makkonen, 1981). This will be particularly important for tangential heat transfer along the cylinder surface, since the surface temperature is in general a function of θ.

The sensible heat flux q_c is given by

$$q_c = h(t_a - t_s), \tag{4}$$

where t_a and t_s are respectively the freestream air temperature and the steady-state accretion surface temperature. The quantity h is the heat transfer coefficient. Both h and t_s are functions of θ, t_s being an unknown solved for by the model, while h must be supplied.

There are insufficient measurements available in the literature to allow one to formulate a general expression for h for icing cylinders. This is one of the major deficiencies of the present model and a fundamental impediment to further progress in the modeling area. However, there are results for h for both smooth and rough cylinders in a cloud-free airstream and these have been used as a basis for the formulation of h in the present model. Some justification for this procedure can perhaps be derived from the fact that the model is concerned only with determining the *initial* rate of icing on the cylinder, and since initially the cylinder is free of ice, heat transfer coefficients for a bare cylinder may be appropriate.

We begin by writing h in terms of the Nusselt number (Nu)

$$h = \frac{k_a \mathrm{Nu}}{D_c}, \tag{5}$$

where k_a is the thermal conductivity of the airstream. Based on the results of Achenbach (1977), Nu may be written approximately as

$$\mathrm{Nu}(\theta) = \mathrm{Re}_c^{0.5}\left[1 - \left(\frac{2\theta}{\pi}\right)^3\right] \tag{6}$$

for smooth cylinders and

$$\mathrm{Nu}(\theta) = \mathrm{Re}_c^{0.5}\{2.4 + 1.2\sin[3.6(\theta - 0.44)]\} \tag{7}$$

for rough cylinders, where $\mathrm{Re}_c = UD_c\rho_a/\mu_a$ is the cylinder Reynolds number. It should be pointed out that Eq. (7) is based on measurements over a very limited range of cylinder Reynolds number, and that the roughness used in Achenbach's experiments bears little resemblance to that encountered on ice accretions. Nevertheless, we have found nothing else in the literature by way of heat transfer measurements from "rough" cylinders. Moreover, neither Eq. (6) nor Eq. (7) allows for the effects of freestream turbulence. In the model, Eq. (6) or Eq. (7) may be specified. In the results presented here, we have used Eq. (7). It should be noted that Nu(θ) described by Eq. (6) has a maximum at 0°, while Nu(θ) from Eq. (7) peaks at 50°. This has a significant influence on the accretion shape under wet conditions, as we shall see later.

In addition to the sensible heat transfer, there is a transfer of latent heat due to the evaporation or sublimation of water vapor from the surface. According to Reynolds' analogy, this term may be written in a similar form to that for the sensible heat transfer, namely,

$$q_e = h\left(\frac{\mathrm{Pr}}{\mathrm{Sc}}\right)^{0.63}\frac{\epsilon l_v}{pc_p}(e_a - e_s), \tag{8}$$

where Pr and Sc are the Prandtl and Schmidt numbers, ϵ the ratio of the molecular weights of water vapor and dry air, p the static pressure in the freestream, c_p the specific heat capacity at constant pressure for dry air, and e_a and e_s the saturation vapor pressure of moist air at t_a and t_s. Finally, l_v is the latent heat of vaporization. If the accretion is dry ($t_s < 0$°C), the latent heat of sublimation might be more appropriate, although even in this case, a film of water may exist on the accretion surface because of the finite time required for the impinging water to freeze completely.

The aerodynamic heating term is given by

$$q_v = \frac{hr_cU^2}{2c_p}, \tag{9}$$

where r_c is the local recovery factor on the cylinder given by

$$r_c = 0.75 + 0.25\cos 2\theta. \tag{10}$$

This latter expression is based on the work of Seban (1960). This term takes into account the adiabatic heating arising from compression of the air which is decelerated in passing around the cylinder, as well as frictional (viscous) heating within the boundary layer. Typically, it becomes significant at the high speeds characteristic of aircraft flight.

The kinetic energy flux of the droplets q_k is given approximately by

$$q_k = \tfrac{1}{2}R_wU^2, \tag{11}$$

where R_w is the droplet mass flux defined by

$$R_w = \beta w U. \tag{12}$$

In Eq. (11) we assume that the droplets are impinging at the freestream airspeed, and further that all of their kinetic energy is converted to heat. This is certainly an overestimate, but since this term is generally small, the error introduced by making such an assumption is probably minor.

The latent heat flux due to freezing of the impinging water is

$$q_f = R_w l_{fs} n, \tag{13}$$

where l_{fs} is the latent heat of freezing at t_s and n the fraction of the accreted mass which freezes. Clearly, $n = 1$ when $t_s < 0°C$ while $n < 1$ when $t_s = 0°C$.

The sensible heat flux between the accretion and the impinging droplets is that required to warm the droplets from the free airstream temperature t_a to the steady-state surface temperature of the deposit, t_s, i.e.,

$$q_w = R_w \bar{c}_w (t_a - t_s), \tag{14}$$

where $\bar{c}_w$ is the average specific heat of water between t_a and t_s. In practice, $\bar{c}_w$ is taken to be a constant in the model, equal to its value at $-10°C$, 4.27×10^3 J kg^{-1} K^{-1}.

Any unfrozen water in a particular sector is assumed to flow into the next downstream sector and participate in the heat exchange there by adjusting to the new steady-state surface temperature of that sector and by freezing in the same proportion as the directly impinging water. Any flow parallel to the cylinder axis is ignored. Because runback water is assumed to leave a sector at the steady-state surface temperature of that sector, its departure does not affect the heat balance equation for the sector it leaves. However, it does affect the heat balance equation for the sector it enters. As the runback water adjusts to the steady-state surface temperature of the sector it enters, it evolves a heat flux given by

$$q_w^* = R_w^* \bar{c}_w (t_s^* - t_s), \tag{15}$$

where R_w^* is the runback mass flux into a sector and t_s^* is the incoming temperature of the runback water. The incoming temperature is assumed to be that of the immediately upstream sector; however, because of the steady state assumption, the existence of runback water implies that t_s^* is 0°C, so that q_w^* is nonzero only at the transition from wet to dry conditions. Also, since R_w^* is the unfrozen portion of the total mass flux of the upstream sector, it may be calculated from

$$R_w^*(\theta_i) = (1 - n_{i-1})[R_w(\theta_{i-1}) + R_w^*(\theta_{i-1})]. \tag{16}$$

Eq. (16) is valid for all but the first and second sectors. There is no runback into the first sector because it is centered on the stagnation line. Moreover, in calculating the runback into the second sector, account must be taken of the fact that half the runback water from the first sector flows upward and half downward around the cylinder. The latent heat evolved by freezing the runback water in sector i is

$$q_f^* = R_w^* l_{fs} n, \tag{17}$$

where n is the same freezing fraction as for the directly impinging water [cf. Eq. (13)].

With the aid of Eqs. (4)–(17), and omitting q_r and q_i, Eq. (3) becomes a nonlinear equation which can be numerically solved within each sector either for the surface temperature t_s in dry growth or for the freezing fraction n in wet growth. In order to do this, e_s must be expressed as a function of temperature. For accuracy and ease of computation we have adopted the saturation vapor pressure formulation proposed by Lowe (1977).

c. *Ice growth*

Having determined the directly impinging supercooled water flux, R_{wi} in Section 2a, and the runback flux R_{wi}^* and freezing fraction n_i in Section 2b, we may calculate the icing flux R_i in any sector very simply according to

$$R_i = n_i(R_{wi} + R_{wi}^*). \tag{18}$$

Assuming radial growth of the deposit in each sector, an ice density ρ_I, and allowing for the curvature of the underlying surface and the resulting "divergent" growth, we note that, the local thickness h_i after an accretion time δt is given by (see Appendix B for derivation)

$$h_i = \frac{2R_i \delta t/\rho_I}{1 + \left(1 + \dfrac{4R_i \delta t}{\rho_I D_c}\right)^{0.5}}. \tag{19}$$

This equation assumes that the icing flux R_i does not change significantly during the interval δt. This in turn means that for strict application of this result, δt must be sufficiently short that the growth of the accretion during δt does not substantially alter the airflow, droplet trajectories, or heat exchange around the cylinder. In practice, we have used Eq. (19) for periods up to several minutes, not so much because we believe that the feedback effects are negligible over such intervals, but because we are presently unable to take them into account. However, recent work by Oleskiw and Lozowski (1982) and by McComber (1982) has shown some progress in taking these effects into account and developing a fully time-dependent icing model, at least for the dry cases. The ice density was assumed to be 890 kg m^{-3}. This may be high and therefore underestimate the accretion thickness in regions of dry, porous growth, particularly in the rime feather growth zone near the edge of dry deposits.

Finally, the model plots h_i as a function of θ_i and interpolates the points to determine a smooth profile shape of the accretion. The local icing mass fluxes can also be summed to determine the total ice mass accreted during δt.

3. Model predictions

Our presentation of model predictions here will be limited to a consideration of icing growth rate at the stagnation line and ice accretion profiles for a few representative cases. Because of the number of parameters which control the icing process (including airspeed, air temperature, liquid water content, cloud droplet size distribution, and cylinder diameter), we will not attempt an exhaustive study on the effects of parameter variation. Instead, we choose to present a few results which indicate the qualitative and quantitative nature of the model predictions. Further results are presented in Part II, where we compare experimental and modeled accretions.

All the model calculations presented in this series of papers were performed using a standard droplet size spectrum with a volume median diameter of approximately 20 μm and f_j values [see Eq. (1)] of 0.06, 0.10, 0.19, 0.29, 0.18, 0.08, 0.05, 0.035, and 0.015 for $j = 1, \ldots, 9$, respectively. This spectrum closely approximates the experimental spectra of Part II. Since the experiments employed a cylinder of diameter 2.54 cm, the model results also refer to a cylinder of this size. Fig. 1 presents the stagnation line growth rate predicted by the model as a function of airspeed and liquid water content for a cylinder 2.54 cm in diameter in an airstream at −15°C. The cusps on the curves represent the transition from dry to wet growth, which occurs at decreasing airspeed as the liquid water content is increased. For the cases presented here, the transition occurs at an almost constant value of the liquid water flux, equal to $(38 \pm 2) \times 10^{-3}$ kg m^{-2} s^{-1} and a roughly constant value of the growth rate. When all of the growth is dry (airspeed < 30 m s^{-1}), the stagnation line growth rate is simply proportional to the liquid water content. In this region it varies almost linearly with airspeed. The increase in fact is somwhat faster than linear because the collision efficiency also increases with airspeed. In the wet growth region (to the right of the cusps), the growth rate is less dependent upon airspeed, especially when the liquid water content is relatively small. There is initially a continuing increase in the growth rate as airspeed increases due to the sensible heat flux term for the impinging water. However, at very high speeds, the growth rate steadies or begins to decline with increasing velocity, because of the effect of aerodynamic heating. Where wet growth occurs for all three liquid water contents (airspeed > 100 m s^{-1}), the growth rate no longer varies linearly with liquid water content. In fact, trebling the liquid water content increases the growth rate by only about 40%.

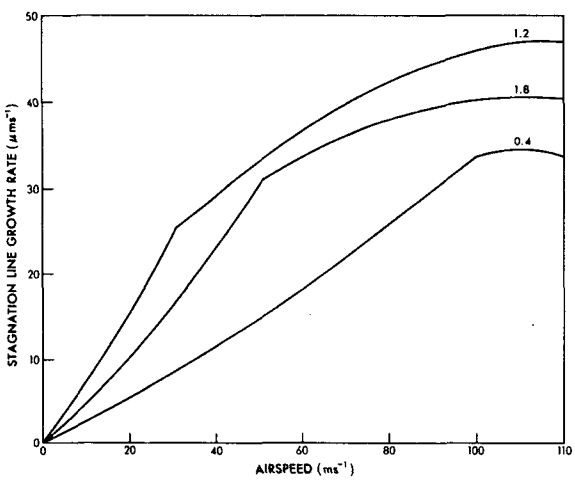

FIG. 1. Stagnation line growth rate predicted by the model at −15°C, for liquid water contents of 0.4, 0.8, and 1.2 g m^{-3}. The cusps on each curve represent the transition between dry growth (to the left) and wet growth (to the right). The cylinder is 2.54 cm in diameter. A cloud droplet spectrum with a volume median diameter of 20 μm was employed.

Figure 2 is similar to Fig. 1 except at −5°C. Comparison of the two figures illustrates the strong influence of temperature on the growth rate in the wet zone (although it has no influence on dry growth). For these conditions, the maximum growth rate occurs at an airspeed of about 70 m s^{-1} and at this speed, the growth rate is relatively insensitive to the liquid water content. Although the graph has not been extended beyond 120 m s^{-1}, the slope of the curves does suggest that at sufficiently high speeds, no icing will occur at the stagnation line. This result is consistent with measurements of ice accretion on helicopter rotor blades (Stallabrass, 1957).

The model-predicted accretion profiles for a number of cases which typify the range of profile types encountered in the experiments (see Part II), are presented in Fig. 3. Values of the liquid water content were nominally 0.4, 0.8, and 1.2 g m^{-3}, but the actual values employed in the model were the same as those measured in the experiments which differed from the nominal values by a few percent. The static pressure is taken to be 100 kPa, although this may be varied if desired. The icing times were chosen to correspond to those of the experiments described in Part II. Unfortunately, these deposits were in general sufficiently large by the end of the interval, that a significant effect on the airflow, cloud water flux and heat transfer might be expected. Thus the model assumption that the icing characteristics do not change over the icing interval, and therefore that the accretion thickness may be estimated by simply extrapolating the initial accretion rate, has to be questioned. All of the model profiles

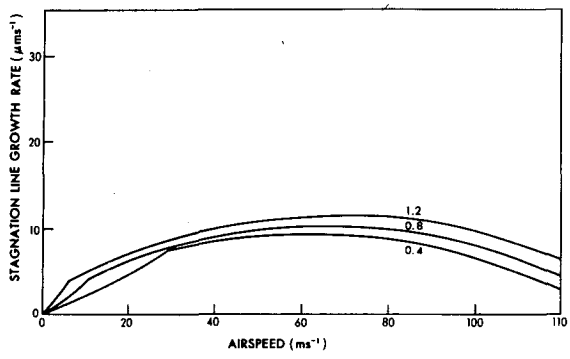

FIG. 2. Stagnation line growth rate predicted by the model at −5°C, for liquid water contents of 0.4, 0.8, and 1.2 g m^{-3}. The cusps on each curve represent the transition between dry growth (to the left) and wet growth (to the right). The cylinder is 2.54 cm in diameter. A cloud droplet spectrum with a volume median diameter of 20 μm was employed.

illustrated were computed assuming the "rough" formulation for the heat transfer coefficient [Eq. (7)]. This has a significant effect on the resulting accretion profiles for the wet cases, for which the ice distribution is strongly influenced by (though not exclusively determined by) the distribution around the cylinder of Nu(θ). In the dry cases, the shape of the accretion is determined by the local collision efficiency and Nu(θ) does not play a role, since the heat transfer is sufficient to allow freezing of all the locally impinging water.

Figure 3 illustrates four different types of profile which occur according to the wetness of the accretion surface. Case A is a dry accretion ($t_s < 0$°C everywhere) and the resulting shape is a smooth crescent, giving the cylinder a somewhat elliptical profile to the flow. Case (B) is wet near the stagnation line and runback occurs to about 25°, beyond which the accretion becomes dry. The result is the development of bulges or horns centered at about 20°. Cases C, D, E, and F are all qualitatively similar inasmuch as runback extends even further around the cylinder than in case B. Thus, instead of forward pointing horns, the development of laterally pointing lobes ("mouse ears") occurs. Finally, case G is so wet that runback to 90° occurs and, by assumption, the unfrozen water at this point is shed into the airstream, thereby leading to an abrupt truncation of the accretion profile at 90°.

In all these cases, the stagnation line regime (wet or dry) can be used to characterize the overall accretion, although in case B and C the accretion becomes dry at some distance from the stagnation line. However, in no case does the stagnation line growth rate appear to be characteristic of the overall growth, since for dry conditions the growth rate at the stagnation line is a maximum, while in wet conditions it is a local minimum.

Although the model is not time-dependent, inasmuch as the icing rates calculated are those which prevail only at the initial instant, a type of pseudo time-stepping can be introduced into the results by examining how the time extrapolation is performed; that is, for calculation of the ice thickness at a particular point on the cylinder surface. At present, the ice thickness in the model is calculated for each angular sector using Eq. (19). Because of feedback between the growing accretion and the mechanics and thermodynamics of the icing process itself, such a simple, linear extrapolation of the initial growth rate can only be valid over very short time intervals (perhaps a few tens of seconds). Thus extrapolation over several minutes as we have done here is questionable.

Suppose instead of extrapolating over the total icing time δt, we extrapolate over $\delta t/n$, where n is some integer such that $\delta t/n$ is at most a few tens of seconds. Then an accretion profile can be drawn, valid at $\delta t/n$. If we now wish to extrapolate for a further $\delta t/n$, we need to estimate new ice accretion rates at the new surface points. In order to do this properly, a new flow field and droplet trajectories must be calculated and a new thermodynamic energy equation solved. The alternative to such an arduous task, is to try to make use of the initial accretion rates $R_w(\theta_i)$ in order to make

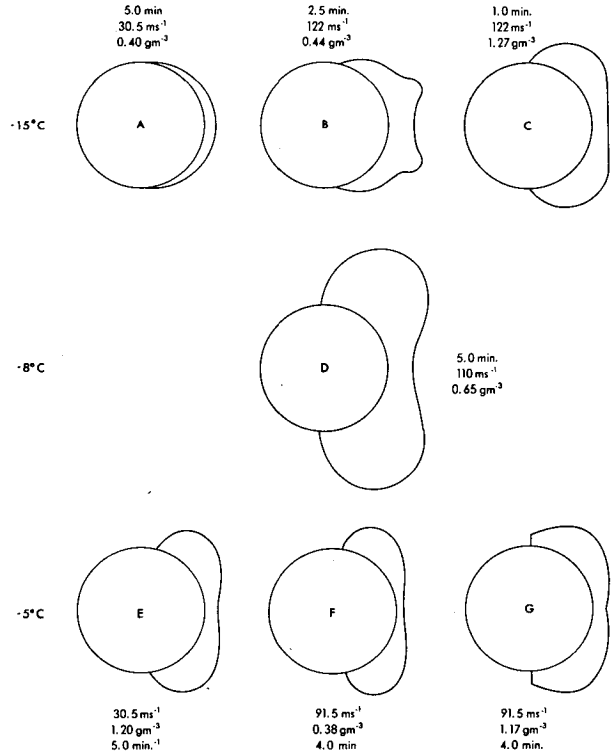

FIG. 3. Model-predicted accretion profiles, under the specified conditions of ambient air temperature (°C), airspeed (m s^{-1}), cloud liquid water content (g m^{-3}) and accretion time (min). These profiles were computed using Eq. (19) and by extrapolating in time in a single step.

a second step or extrapolation. One way to do this is to continue to use R_{wi} at θ_i, i.e., assume that at a given angle measured relative to the original cylinder, the initial accretion rate used to calculate the ice thickness for the first step, can be used again to calculate the ice thickness for the second step. Proceeding in this way for n steps is identical to making a single step extrapolation over the entire interval δt.

A different approach might be to apply the initial icing rates already computed for the first step, not at the same angle relative to the cylinder, but at the same distance along the accretion surface, using now the new accretion surface as the baseline rather than the original cylinder surface. We cannot justify this multistep extrapolation approach formally, nor is it possible to contend that it is the optimum extrapolation method, given that only initial icing rate data are available. However, we feel that it is worth exploring, and its value can best be determined, *post facto,* through comparison with experiments (see Part II).

Figure 4 shows some of the accretion profiles of Fig. 3, re-computed using this technique. The application of the extrapolation algorithm was accomplished by hand, so that the resulting profiles are not generated as automatically as those of Fig. 3, nor are they quite as objective, since they are not machine computed and drawn. For case A, the pseudo-time dependent approach leads to no significant difference from the single step extrapolation. On the other hand, for the large, wet accretions, significant differences do occur. The stagnation line depressions tend to become more pronounced, as a result of the lobes being moved more forward and reduced in size. The stagnation line thickness itself remains unchanged. This is unrealistic inasmuch as the flattening or hollowing of the stagnation line region would be expected to reduce the stagnation line collision efficiency and thus enhance the depression. Moreover, the heat transfer at the lobes would probably be higher because of their smaller radius of curvature, while water shedding from the lobes themselves would probably reduce the accretion thickness behind the lobes. Stochastic effects might also be expected to make the accretion three-dimensional with variation along the cylinder axis. Thus the computed profiles can only be expected to be representative in an average sense.

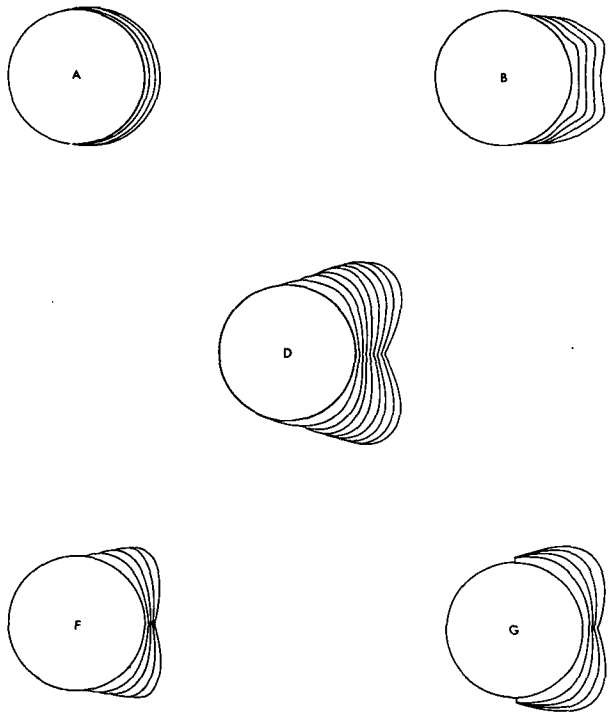

FIG. 4. Model predicted accretion profiles under the conditions specified in Fig. 3 for the corresponding case (A, B, D, F, G). These profiles were computed using the pseudo-time dependent approach discussed in the text. In case A, three equal time steps were used, in cases B, F, and G, four steps, and in case D, eight steps. The profiles are shown after each step. The total accretion interval for each case is the same as in Fig. 3.

4. Summary and conclusions

The model presented in this paper represents a significant improvement over previously published attempts to quantify icing on non-rotating cylinders. Unlike previous models, it is not constrained to a consideration of stagnation line conditions only, nor is it necessary to limit its application to cases where the accretion is growing dry. By calculating the impinging cloud water fluxes as a function of angle around the cylinder and by solving the heat balance equation to determine the local thermodynamic conditions at the accretion surface, we have derived a simulation model of more general applicability. At this point, it is possible to say that the model is qualitatively realistic (see Part II for a quantitative appraisal), inasmuch as it predicts and takes into account surface runback of unfrozen water, and it is capable of simulating qualitatively at least certain well-known icing features such as "spearhead" and "horned" growth, stagnation line depressions and runback lobes. Finally, although the model is not strictly a time dependent one, a pseudo-time dependence can be introduced, which may be a more realistic way to extrapolate the initial growth rates in time than by making a single growth step.

Applications of this model to specific icing situations are likely to require even further development because of additional constraints imposed by the nature of the accreting substrate. For example, applications to power line icing should allow for the possibility of twist in the conductor as gravity begins to act on the developing accretion. Applications to helicopter rotor blade icing will need to make the geometrical transition to an airfoil rather than a cylindrical substrate, but the fun-

damental physics will remain the same as that incorporated into the present model. Of course, blade oscillation and centrifugal effects also will have to be taken into account. However, the model will likely have its most satisfactory application as a means of quantifying icing *potential* for these and other applications. Icing on one or more cylinders of various sizes can be used as a basis for assessing or predicting icing effects on other structures, be they on the ground, the ocean, or in the air. Thus the prediction of cylinder icing is fundamental to understanding and assessment in all branches of icing research. It is hoped, therefore, that the present model will contribute, in a modest way, to the unifying of the overall icing effort in whatever area it may happen to be.

This is not to suggest that the present model is without need for improvement. On the contrary, it could be significantly improved in several ways

1) by incorporation of an improved formulation for the "rough" heat transfer coefficient. This is particularly important as it is apparent from the model predictions that the occurrence and location of horned lobes is largely influenced by the angular dependence of the Nusselt number, which in turn is determined by surface roughness and airstream turbulence,

2) by adding the physical processes of splashing, and shedding of runback water from protuberances at other than 90°,

3) by allowing for internal heat conduction or surface heating by de-icing or anti-icing devices and

4) by making it truly time-dependent, encompassing feedback effects between the growing accretion and the airstream.

Acknowledgments. One of the authors (EPL) is indebted to the National Research Council of Canada and to the University of Alberta, which jointly, through the provision of a study leave program, made it possible for him to become involved with this work. We would like to acknowledge the contributions of Mr. J. T. Cansdale of RAE Farnborough and Dr. J. Shaw of NASA Lewis, with whom we have had stimulating discussions concerning the modeling of icing. Thanks are due to Ms. L. Smith who typed the manuscript and to Mr. G. Lester and his staff who prepared the illustrations. Finally, we wish to thank Dr. L. Makkonen and two other anonymous referees for their helpful comments.

APPENDIX A

Details of the Local Collision Efficiency Calculation

The formulas for determining the local collision efficiency for each drop size are based on the equations and tabulated results of Langmuir and Blodgett (1946). These results were obtained using a differential analyzer. Recent verification of their numerical results using a digital computer to calculate water droplet trajectories (e.g., Oleskiw, 1981), has revealed that they are quite dependable. In most instances, the formulas proposed by Langmuir and Blodgett to fit their numerical data have been used. In some cases, however, it was felt that a better fit to their numerical data could be obtained by adopting somewhat different formulas.

One begins by computing for each droplet category its Reynolds number Re_j, and its Langmuir inertia parameter K_j, according to

$$\mathrm{Re}_j = \frac{D_j U \rho_a}{\mu_a}, \tag{A1}$$

$$K_j = \frac{\rho_w U D_j^2}{9 \mu_a D_c}, \tag{A2}$$

where ρ_a and ρ_w are the density of the air and water, and μ_a is the dynamic viscosity of the airstream. A modified inertia parameter is then calculated according to

$$K_{0j} = 0.125 + \frac{(K_j - 0.125)}{1 + 0.0967\ \mathrm{Re}_j^{0.6367}}. \tag{A3}$$

With the use of K_{0j}, values of the stagnation line collision efficiency β_{0j}, the total collection efficiency E_j and the maximum impingement angle θ_{mj} are calculated according to

$$\beta_{0j} = E_j = \theta_{mj} \quad \text{for} \quad K_{0j} < 0.125, \tag{A4}$$

$$\beta_{0j} = \frac{1.4(K_{0j} - 0.125)^{0.84}}{1 + 1.4(K_{0j} - 0.125)^{0.84}} \quad \text{for} \quad 0.125 \leqslant K_{0j} \leqslant 7.5, \tag{A5}$$

$$\beta_{0j} = \frac{K_{0j}}{1 + K_{0j}} \quad \text{for} \quad 7.5 \leqslant K_{0j}, \tag{A6}$$

$$E_j = 0.489(\log_{10} 8K_{0j})^{1.978} \quad \text{for} \quad 0.125 \leqslant K_{0j} < 0.9, \tag{A7}$$

$$E_j = \frac{K_{0j}}{\pi/2 + K_{0j}} \quad \text{for} \quad 0.9 \leqslant K_{0j}, \tag{A8}$$

$$\theta_{mj} = \tan^{-1}[1.7(K_{0j} - 0.125)^{0.76}] \quad \text{for} \quad 0.125 \leqslant K_{0j} \leqslant 10, \tag{A9}$$

$$\theta_{mj} = \tan^{-1} K_{0j} \quad \text{for} \quad 10 \leqslant K_{0j}. \tag{A10}$$

Since these formulas are empirical fits to Langmuir and Blodgett's numerical or graphical data, a word about errors is appropriate. A comparison between results obtained using these formulas and the published numerical or graphical data show maximum errors of

0.053, 0.056 and 2.5° for β_0, E, and θ_m. This error analysis covered the range $0.2 \leqslant K \leqslant 100$ and $0 \leqslant \phi \leqslant 10^4$, where ϕ is the Langmuir and Blodgett impingement parameter defined according to

$$\phi = \frac{9\rho_a{}^2 UD_c}{\mu_a \rho_w}. \tag{A11}$$

Finally, the local collision efficiency around the upstream face of the cylinder is evaluated using

$$\beta_j(\theta_i) = \beta_{ij} = \beta_{0j}\cos\left(\frac{\pi}{2}\frac{\theta_i}{\theta_{mj}}\right) + \frac{\pi^3}{\theta_{mj}^3(\pi^2 - 4)} \times \left(E_j - \frac{2\theta_{mj}\beta_{0j}}{\pi}\right) \times \theta_i{}^2 \sin\left(\pi\frac{\theta_i}{\theta_{mj}}\right) \quad \text{for} \quad \theta_i < \theta_{mj},$$

$$\beta_j(\theta_i) = \beta_{ij} = 0 \quad \text{for} \quad \theta_i \geqslant \theta_{mj}. \tag{A12}$$

The form of this empirical equation was chosen to fit the results of a detailed and lengthy calculation of $\beta(\theta)$ performed according to the procedure devised by Langmuir and Blodgett. It satisfies the physical constraints

$$\left.\begin{aligned} \beta_j(0°) &= \beta_{0j} \\ \beta_j(\theta_{mj}) &= 0 \\ \int_0^{\theta_{mj}} \beta_j(\theta)d\theta &= E_j \end{aligned}\right\}. \tag{A13}$$

APPENDIX B

Derivation of Equation (19)

Let $R(\theta, t)$ be the icing flux at time t and angle θ relative to the original cylinder. Let $h(\theta, t)$ be the radial thickness of the ice deposit at t and θ. Then the rate of accretion mass increase in a sector of narrow angular width $\delta\theta$ and unit length along the cylinder axis is

$$\frac{dM}{dt} = R(\theta, t)[r_c + h(\theta, t)]\delta\theta, \tag{B1}$$

where r_c is the cylinder radius. Integrating Eq. (B1) over the interval $0 \leqslant t \leqslant \tau$, we have

$$M(\tau) = \int_0^\tau R(\theta, t)[r_c + h(\theta, t)]\delta\theta dt. \tag{B2}$$

By simple geometry, we may also write the following expression for $M(\tau)$

$$M(\tau) = \rho_I\{[r_c + h(\theta, \tau)]^2 - r_c{}^2\}\frac{\delta\theta}{2}, \tag{B3}$$

where ρ_I is the ice density (assumed independent of θ and t). Equating these results for $M(\tau)$, leads to

$$h^2(\theta, \tau) + 2r_c h(\theta, \tau) - \frac{2}{\rho_I}\int_0^\tau R(\theta, t) \times [r_c + h(\theta, t)]dt = 0. \tag{B4}$$

In order to obtain an explicit solution for $h(\theta, \tau)$, it is necessary to evaluate the integral in Eq. (B4). This can only be done approximately at present because we do not know exactly how R and h vary with time. Thus, we approximate the integral by writing $R(\theta, t) \approx R(\theta, 0)$ and $h(\theta, t) \approx h(\theta, 0) = 0$. This is not a very satisfactory approximation, unless $h \ll r_c$. However, it is consistent with approximating $R(\theta, t)$ at $t = 0$. Integrating and solving the quadratic, we obtain

$$h(\theta, \tau) \approx \frac{2R(\theta, 0)\tau/\rho_I}{1 + \left(1 + \frac{2R(\theta, 0)\tau}{\rho_I r_c}\right)^{1/2}}, \tag{B5}$$

which is essentially Eq. (19).

If instead of assuming $h(\theta, t) \approx h(\theta, 0)$, we consider that perhaps h may vary linearly with time, then we might instead write

$$h(\theta, t) \approx h(\theta, \tau)t/\tau. \tag{B6}$$

Substitution of this approximation into Eq. (B4) along with the previous approximation for $R(\theta, t)$, leads to the result

$$h(\theta, \tau) \approx \frac{R(\theta, 0)\tau}{\rho_I}. \tag{B7}$$

Clearly Eqs. (B5) and (B7) yield the same result in the limit as $\tau \to 0$. We have found that over the short time intervals considered in our experiments, the model predictions differ insubstantially whether one uses Eq. (B5) or Eq. (B7). Over longer time intervals, the differences can be large, but then it is probably not valid to assume that $R(\theta, t) \approx R(\theta, 0)$ over such long intervals. Thus in these cases, both equations probably will yield erroneous predictions.

REFERENCES

Achenbach, E., 1977: The effect of surface roughness on the heat transfer from circular cylinders to the cross flow of air. *Int. J. Heat Mass Transfer,* **20,** 359–369.

Ackley, S. F., and M. K. Templeton, 1979: Computer modelling of atmospheric ice accretion. Rep. CRREL 79-4, U.S. Army Cold Regions Res. and Eng. Lab., 36 pp.

Cansdale, J. T., and I. I. McNaughton, 1977: Calculations of surface temperature and accretion rate in a mixed water droplet/ice crystal cloud. Royal Aircraft Establishment Tech. Rep. 77090, 24 pp.

Langmuir, I., and K. B. Blodgett, 1946: A mathematical investigation of water droplet trajectories. *Collected Works of I. Langmuir.* Pergamon Press, **10,** 348–393.

List, R., 1977: Ice accretions on structures. *J. Glaciol.,* **81,** 451–465.

Lowe, P. R., 1977: An approximating polynomial for the computation of saturation vapor pressure. *J. Appl. Meteor.,* **16,** 100–103.

Lozowski, E. P., and R. d'Amours, 1980: A time-dependent numerical model for spherically symmetric hailstone growth thermody-

namics under constant ambient conditions. *J. Atmos. Sci.*, **37**, 1808–1820.

——, and M. M. Oleskiw, 1981: Computer simulation of airfoil icing without runback. Pap. AIAA-81-0404, Amer. Inst. of Aeronaut. and Astronaut. 8 pp.

——, J. R. Stallabrass and P. F. Hearty, 1979: The icing of an unheated non-rotating cylinder in liquid water droplet-ice crystal clouds. National Research Council of Canada Report LTR-LT-96, 61 pp. [Available from NRCC, Ottawa, Canada, K1A 0R6.]

Ludlam, F. H., 1951: The heat economy of a rimed cylinder. *Quart. J. Roy. Meteor. Soc.*, **77**, 663–666.

Makkonen, L., 1981: Estimating intensity of atmospheric ice accretion on stationary structures. *J. Appl. Meteor.*, **20**, 595–600.

McComber, P., 1982: Numerical simulation of ice accretion on cables. *Proc First Int. Workshop on Atmospheric Icing of Structures*, CRREL, Hanover, NH.

Messinger, B. L., 1953: Equilibrium temperature of an unheated icing surface as a function of airspeed. *J. Aeronaut. Sci.*, **20**, 29–41.

Oleskiw, M. M., 1981: A computer simulation of time-dependent rime icing on airfoils. Ph.D. thesis, The University of Alberta, 302 pp.

——, and E. P. Lozowski, 1982: The design and testing of a Lagrangian computer model for simulating time-dependent rime icing on two-dimensional structures. *Proc. First Int. Workshop on Atmospheric Icing of Structures*, CRREL, Hanover, N.H.

Seban, R. A., 1960: The influence of free stream turbulence on the local heat transfer from cylinders. *J. Heat Transfer*, **82**, 101–107.

Stallabrass, J. R., 1957: Icing flight trials of a Bell HTL-4 helicopter. National Research Council of Canada Report NRC-NAE-LR-197. [Available from NRCC, Ottawa, Canada, K1A 0R6.]

Stallabrass, J. R., 1980: Trawler icing: A compilation of work done at NRC. National Research Council of Canada Report DME-MD-56, 113 pp. [Available from NRCC, Ottawa, Canada, K1A 0R6.]